Investigation of five types of switchable retroreflector films for enhanced visible and infrared conspicuity applications

P. Schultz, B. Cumby, and J. Heikenfeld*

University of Cincinnati, Novel Devices Laboratory, School of Electronic and Computing Systems, Cincinnati, Ohio, USA

*Corresponding author: heikenjc@ucmail.uc.edu

Received 7 February 2012; revised 26 March 2012; accepted 28 March 2012;
posted 29 March 2012 (Doc. ID 161876); published 4 June 2012

We report on the physics, design, characterization, and demonstration of five viable techniques for switchable retroreflectors, including integrated electrowetting scattering, integrated and external electrowetting light valves, external liquid crystal light valve, and external liquid crystal scattering. All techniques were evaluated for use in conspicuity applications spanning wavelengths in the visible and IR (night vision). Achieved performance includes high optical efficiencies up to nearly 30% (out of a maximum 35%), visibly fast switching speeds of <100 ms, low to moderate operating voltages ranging from 5 to 60 V, more than ±45 deg of operation angle, and implementation with pressure-sensitive, adhesive-backed films of 0.7 to 1 mm thickness for flexibility and impact resistance. Each approach has unique strengths and weaknesses, which will also be discussed for applications ranging from commercial to military conspicuity.

OCIS codes: 230.0230, 230.2090, 230.4110, 230.4000, 260.3060.

1. Introduction

Retroreflectors are commonplace in conspicuity and range-finding applications, as they efficiently and predictably reflect light back to the source. By modulating (flashing) this retroreflected light, conspicuity can be revealed or hidden on demand. The majority of prior work in switchable retroreflectors has involved modulation by micro-electromechanics [1,2] or quantum wells [3]. These systems exhibit data rates up to 45 Mbps [4], with long distance links of up to 16 km [5], all achieved in a small and highly portable package. However, these previous approaches are not suitable for naked-eye conspicuity applications. The ideal requirements for naked-eye conspicuity are numerous: (1) wide visible spectral range for a bright reflection (full width half maximum of >100 nm); (2) on/off contrast of ideally >10:1; (3) large reflective area (>100 cm^2) for ease of viewing at a distance and for ease in aligning interrogating sources such as lasers; (4) flexible tape-like form factors for application to curved surfaces, the flexibility also ideally allowing impact resistance; (5) wide input angle to eliminate the need to precisely orient the retroreflective surface; (6) switching at speeds as fast as the human eye response (<100 ms) to maximize recognition (as opposed to a slow gradual switch that does not draw attention); (7) low modulation power, in some cases even battery operation for mobile/remote placement; (8) high optical efficiency such that retroreflected brightness far exceeds the intensity of reflection from diffusely reflecting surroundings.

This article broadly investigates and compares electrically-modulated retroreflector film technologies for rapid visual identification. Five switching techniques based on electrowetting and liquid crystal technologies were fabricated and tested. This article first describes the retroreflector platform selection, then analyzes in detail the physics, design, and characterization of the five chosen modulation methods. A final comparison and discussion is also provided to prioritize the technologies for further development.

1559-128X/12/173744-11$15.00/0

A field test demonstration is also performed to validate long-range capability, and capability in the dark using IR (night vision). This article provides significant progress toward adapting switchable retroreflector technology to a wide variety of conspicuity applications.

2. Choosing the Retroreflecting Optical Film

The common optical element across all five investigated platforms is a base retroreflective layer. There are three general types of retroreflectors [6] which, chronologically in order of commercial introduction, are: glass bead, corner cube, and full cube. The first task for this work was to determine which base retroreflector layer to utilize. Table 1 provides the key parameters considered in selection. Each type of retroreflector is now briefly introduced.

Glass bead type retroreflectors were the first developed and are also known as "Engineer Grade Sheeting." This lowest-cost type of retroreflector uses glass beads with diameters in the microscale, partially embedded in a metalized reflective backplane. At the input surface of the bead, the incident light is refracted in a direction path close to the center of the back of the bead. The light reflects back to bead's surface and is refracted again upon exiting the bead, parallel to the incident light. Optical efficiency, which is also known as retroreflectivity, is the percent of incident light being reflected back to the source. Glass bead suffers from high surface reflections (loss) and lower overall efficiency of about 15% [6,8]. Glass bead retroreflectors do, however, provide the widest input angle, especially with use of high refractive index glass.

Corner cube retroreflectors [9,10] can be realized as an array of truncated corners of orthogonal cubes. They offer high efficiency while covering half of a hemisphere of input angles. Corner cubes can be inexpensively microreplicated in large area polymer films. Also, corner cubes provide a built-in cavity into which the switching element can be integrated. Their physics of operation will be discussed later in this section.

Full cube retroreflectors are the newest type of retroreflective structure, and were introduced in 2006 by 3M under the name Diamond Grade DG^3. These offer the highest efficiency of about 58% [8,11], but are not as widely available as their counterparts. Furthermore, the retroreflection is not maintained for all orientations (rotations of retroreflecting surface).

After evaluation for efficiency, maximum input angle to the retroreflective surface, the ability for switching integration in the retroreflector, and allowance for arbitrary orientation (Table 1), corner cube retroreflectors were determined to be the platform for this work. Photos and data for a typical corner cube retroreflector are shown in Fig. 1. The three

Table 1. Base Retroreflector Technology Comparison [6,7]

	Bead	Corner Cube	Full Cube
Efficiency	15%	35%	58%
Max input angle at 30% of max refl.	±60°	±45°	±30–38°
Internal switching integration	No	Yes	No
Arbitrary orientation	Yes	Yes	No

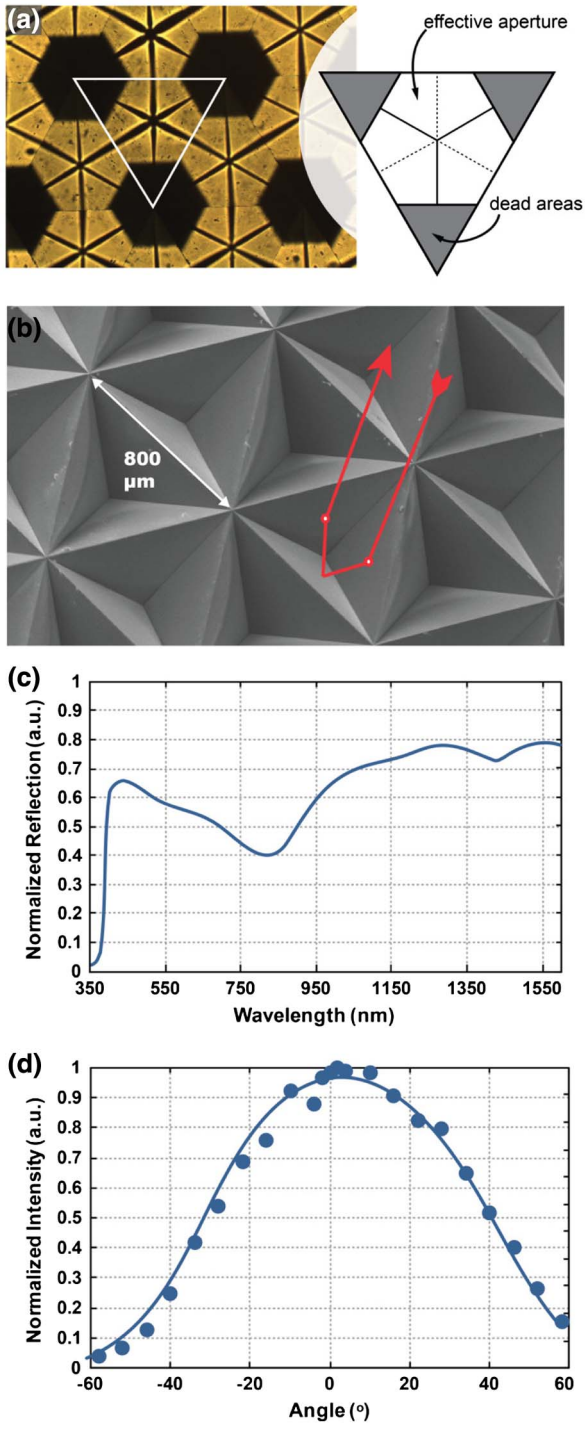

Fig. 1. (Color online) Corner cube retroreflectors: (a) top view of a corner cube retroreflector which visually reveals the retroreflecting and dead areas, (b) SEM of corner cube structures and diagram of an example retroreflection path (not an actual ray trace), (c) retroreflection vs. wavelength from 350 to 1600 nm, (d) retroreflection as a function of input angle as measured using the experimental setup in Fig. 3(b) of [19]. Points are experimental data; trend curve is for guidance.

sidewalls have a slope of 54.74°, and when incident light reflects off all three sidewalls it will achieve retroreflection [Fig. 1(b)]. As also seen in Fig. 1(a), the optically active aperture is an equilateral triangle, outside of which exist dark areas at the three corners. These dark spots represent ~35% of the total area of the corner cube, and are where incident light reflects off only two sidewalls. A retroreflective film such as Reflexite V82 (used in this study) exhibits the following properties: the retroreflection of a collimated light reduces to ~50% intensity within a ±0.2° observation cone, and is effectively nonobservable (<1%) past ~ ± 2°. The reflection as a function of wavelength covers the entire visible spectrum and into the IR, as shown in Fig. 1(c). The input angle ($\theta_{30\%}$) is ±45°, defined in this work as the largest angle of incident light before retroreflected intensity reduces to 30% of its maximum [Fig. 1(d)]. There exists more advanced theoretical understanding for retroreflectors, such as bidirectional reflectance distribution function, which is included herein by reference [12–14].

In this study, two particular corner cube structures were utilized. In some cases, Reflexite V82 film (175 μm sidewall length) was used behind an optically modulating layer [top view, Fig. 1(a)]. When the optical modulation was to be integrated within the corner cubes themselves, a custom microreplicated corner cube surface was also provided by Reflexite [800 μm sidewall length, angled view SEM image of Fig. 1(b)].

3. Selection of Electrical Modulation Methods

Several reflective optical switching technologies [15] can satisfy the ideal requirements described in the introduction section. Electrophoretic display technology could be used, but only the in-plane variations have the possibility of being transparent, and are too slow to match the human eye response. Electrochromic technology is operable with low voltage, and provides an excellent transmissive state, but commercial devices also switch very slowly (100's ms to 10's of s). Cholesteric liquid crystal provides excellent transparency, but cannot modulate over the entire visible spectrum. At the time of this work, it was determined that the most appropriate modulation techniques were based on electrowetting [16] or more conventional liquid crystal technology [17–19]. Both of these technologies can switch quickly, can modulate over the entire visible spectrum and into the IR, and can operate with little angular dependence.

A. Electrowetting

Electrowetting will only be reviewed in brief as a complete review can be found elsewhere [16]. Electrowetting uses electromechanical force to reduce liquid contact angle on a dielectric surface. This can be described by the well known electrowetting equation: $\cos\theta_V = \cos\theta_Y + CV^2/2\gamma_{CI}$, where θ_V is the voltage induced contact angle, θ_Y is Young's angle (at 0V), C is the capacitance per unit area of the hydrophobic surface (F/m^2), V is the applied voltage, and γ_{CI} is the interfacial surface (N/m) tension between conducting fluid (often water) and insulating fluid (often oil). The polar fluid serves as one electrode. The dielectric covers a counter electrode, and is always hydrophobic (often an insulating polymer covered with a hydrophobic fluoropolymer). As will be seen in later sections, electrowetting can be applied to change optical transmission [20] or refraction [21]. The speed of operation can be as fast as a few ms for devices of <100 μm in size. Operation voltages can range from 10–100 V based on materials used (C, γ_{CI}).

B. Liquid Crystal

A general description of liquid crystal technology can be found elsewhere [17–19]. Liquid crystals have been used extensively in the display industry as the preferred method of pixel switching in consumer televisions and monitors (LCDs), as well as smart windows with polymer dispersed liquid crystal sheets (PDLC). Liquid crystal systems are highly developed and well understood and cost is continually decreasing. Some types of liquid crystal devices are highly transparent and can provide high contrast ratios over a wide spectrum. Liquid crystal devices can operate from low to moderate voltages (<5 to 40 V, based on thickness) and have fast switching speeds (typically 10's of ms).

4. Optical Efficiency Model

For all approaches reviewed herein, the incident light must transmit through the modulation layer, retroreflect, and then pass back through the modulation layer a second time. If the modulation layer is inefficient, the compounded optical losses will significantly reduce the observable contrast ratio.

Optical transmission through each layer can be expressed as ($T_n = 1 - \alpha_{mat} - R_n$), where α_{mat} is the material's optical absorption coefficient, and R_n is the material's Fresnel reflectance due to refractive index mismatch with adjacent layers. The Fresnel reflectance will be calculated for normal incidence as $R \cong (n_1 - n_1/n_1 + n_2)^2$. The product of adjusted transmissions of all the layers provides a total single optical pass transmittance of $T = T_1 \cdot T_2 \ldots \cdot T_n$, where T_n is the transmittance of each layer. To get a quantity for the full efficiency with retroreflection, the light must travel through the modulating device twice (T^2). Depending on the modulation device, there is also an associated transmissive aperture (a_{MD}), and light outside this transmissive aperture is lost. The retroreflector returns the light parallel to the incident light, but not at the same location; therefore, when the modulating layer is external (not integrated inside the corner cube), the worst-case transmissive aperture should be calculated as (a_{MD}^2). There is also the associated efficiency with the retroreflector itself (ρ_{RR}). For the corner cube retroreflectors tested herein, due to manufacturing

imperfections, additional Fresnel losses, 90% reflective Al, and a retroreflective aperture of 65%, a final efficiency of $\rho_{RR} = 35\%$ is typically achieved.

The total retroreflective efficiency combines all the losses discussed above, and can be expressed as:

$$\eta(\%) = T^2 \cdot a_{MD}^2 \cdot \rho_{RR} \quad (1)$$

At this point, the reader is now ready for review of the various devices tested in this work.

5. Electrowetting Lenslet Scattering

Our research group began investigating switchable retroreflectors in 2007, and therefore this will be the first device topic reviewed. These devices rely on electrowetting lenslets [22] that are integrated into the corner cubes themselves.

A. Fabrication and Construction

The electrowetting lenslet retroreflector is shown in Fig. 2. Detailed information on the fabrication and operation of this device is provided elsewhere [22,23]. The device consists of a corner cube retroreflector backplane that has been coated with electrowetting films and dosed with oil and water. These immiscible fluids create a concave shaped meniscus, which creates a concave lens because the oil has a refractive index of >1.4 and the water has a refractive index of 1.3. To allow ease of fabrication, the larger, 800 μm corner cubes were utilized.

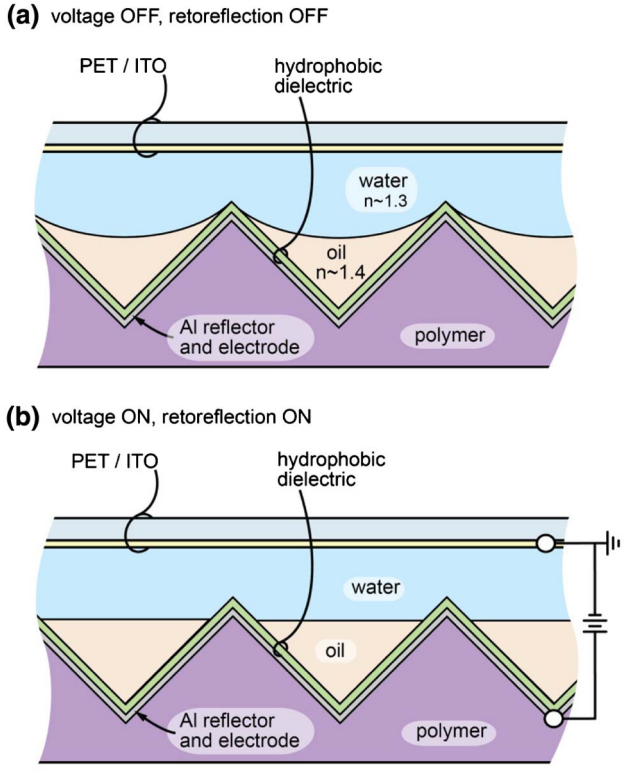

Fig. 2. (Color online) Electrowetting lenslet retroreflector (a) in the scattering (voltage off) state, (b) with voltage provided to enable the retroreflecting/on state.

B. Electrical Switching

Once the device is fully assembled, and for the case of no applied voltage (off state), the meniscus at the oil and water interface is concave. This can be seen in Figs. 2(a) and 3(a). In this state, light incident onto the electrowetting retroreflector will be refracted as it passes through the meniscus, and therefore be optically scattered. The device therefore appears as a diffuse reflector (inconspicuous).

Figures 2(b) and 3(b) show the device when electrically powered. Electrowetting reduces the water contact angle with the hydrophobic dielectric. With application of ~19 V, the water contact angle reaches ~125 deg, the meniscus becomes flat, and the device behaves like a conventional retroreflector. If the applied voltage is increased even more, the meniscus will become convex, creating a second diffusely scattering state. Typically, the voltage is not increased further (instead, voltage is simply set back to zero to create the diffuse state).

C. Retroreflection Results

The retroreflection input angle, as a function of the light source's incident angle, is shown in Fig. 4. For this device, greater than 10:1 contrast ratio was achieved out to ±30°. The maximum input angle at 30% of maximum reflection ($\theta_{30\%}$) is at 30°–35°, and can be increased by use of higher refractive index oils with little to no loss to the electrical operation of the device. Uncharacteristic (for a basic retroreflector) dips and peaks in reflection can be seen for ~ ± 10° and ~ ± 20°, which is speculated to be due to thin film interference from the hydrophobic dielectric stack [23].

The electrowetting lenslet retroreflector uses a method of modulation that is integrated within the corner cube structure itself. This lends itself to slightly more difficult fabrication, but requires fewer deposited layers (less optical loss), and makes the device thinner (and potentially more flexible as a result). The approximate single-pass transmission is calculated to be about $T = 87.8\%$. Since there are no layers to limit the active area of the modulation device, the active area for modulation (a_{MD}) is 100%. The fixed optical efficiency of the retroreflector with Al reflection and retroreflective aperture is $\rho_{RR} = 35\%$.

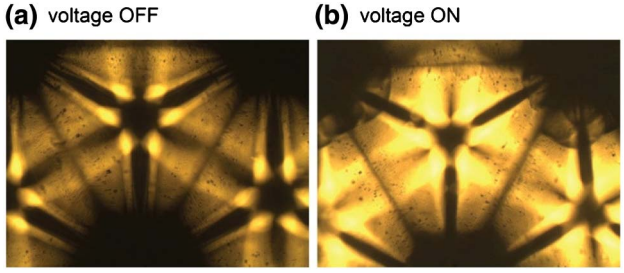

Fig. 3. (Color online) Collinear images of the lenslet retroreflectors with (a) voltage off and retroreflection off, (b) voltage on and retroreflection on. The image intensities are not comparable (the camera sensitivity was adjusted to obtain good images for the off and on states).

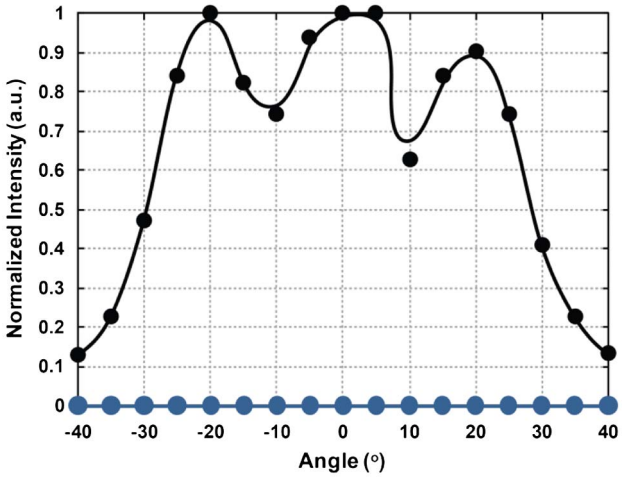

Fig. 4. (Color online) Retroreflection as a function of input angle for integrated electrowetting lenslets. Both states of operation are plotted. Points are experimental data, and trend curves are for guidance.

As a result, the total retroreflective efficiency is $\eta(\%) = 27\%$.

D. Discussion

The approach of integrating the electrowetting lenslet inside the retroreflector has several advantages. The operating voltage can be lower than a conventional electrowetting lens [24] because a contact angle change of only 55 deg is needed to flatten the meniscus. The energy per switch is also very low ($\sim$1.8 mJ/m^2) because the water only touches $\sim$48% of the total device area for the electrowetting capacitor. Based on the simple materials used, it will be seen that the optical efficiency is the highest of those described herein. As reported previously [22], scaling the corner cubes to 10 μm could result in very fast switching speeds of $<$0.1 ms, which far exceeds the response time of the human eye. The spectral range covers the entire visible spectrum, and the input angle is wide. A large total reflective area is possible ($>$100 cm^2) and the entire device can be thin and flexible. Fast switching speed may be the most significant advantage over the other investigated approaches, the next of which will now be reviewed.

6. External Electrowetting Light Valve

Electrowetting light valves were first reported in 2003 [25] and are now close to commercialization for video-rate reflective displays (LiquaVista/Samsung). Electrowetting light valves are highly optically efficient in transmissive or reflective mode [20, 25–27], and therefore initially appear as a strong candidate for modulating retroreflection. The simplest way to integrate electrowetting light valves and a retroreflector is to fabricate them as separate components, and simply epoxy/laminate them together.

A. Fabrication and Construction

The external electrowetting light valve retroreflector can be seen in Fig. 5. The construction is a large pixel

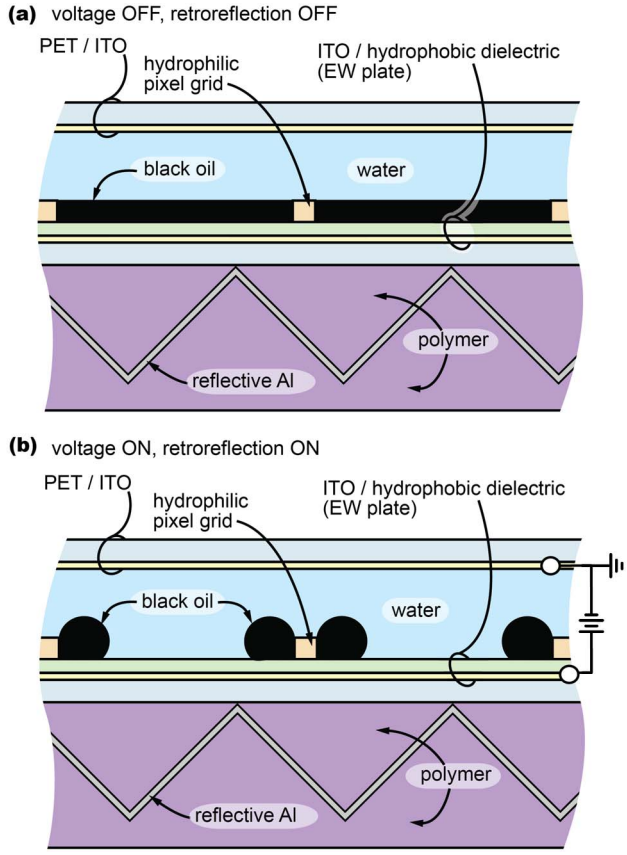

Fig. 5. (Color online) External electrowetting light valve retroreflector in the (a) voltage off state and light absorbing state, (b) voltage on state and retroreflecting state.

array of electrowetting light valves, but using a common electrode for all pixels such that the entire film switches on/off uniformly. Complete details of our process for pixel array fabrication can be found elsewhere [20].

B. Electrical Switching

Figures 5(a) and 6(a) show the zero voltage state of the device. In the off state, the oil (which is hydrophobic) forms a film that fully covers the hydrophobic dielectric. The oil contains $\sim$10 wt.% of black dye [20] which absorbs the incident light, thereby reducing the retroreflection. Most of the light transmitting through the pixel array in the zero voltage state is due to light leakage through the hydrophilic pixel grid. This light leakage can be reduced through use of a black photoresist (not demonstrated herein, but available commercially as MicroChem XP Black SU-8 [27]).

The switching on of the electrowetting pixels involves a single application of $\sim$15 V and two resulting fluid mechanisms. First, a vertical electromechanical force overcomes interfacial surface tension force and breaks up the oil film such that the water contacts the hydrophobic dielectric. Once in contact, a horizontal electromechanical force displaces the oil to the ends of the pixels (electrowetting), creating a transmissive aperture, thereby allowing retroreflection

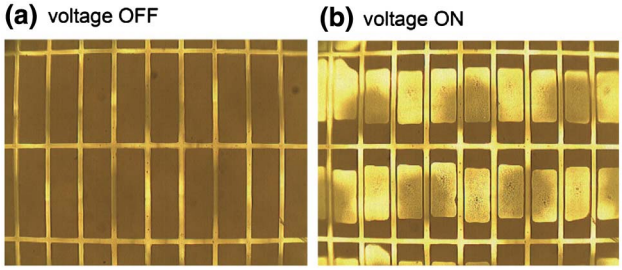

Fig. 6. (Color online) Collinear images of the external electrowetting light valve retroreflector in the (a) voltage off state, (b) voltage on state.

[Figs. 5(b) and 6(b)]. A complete study of the predictive nature of the oil film breakup mechanism can be found elsewhere [26]. When the voltage is removed, the oil film suppresses retroreflection by rapidly recovering (10's ms) the hydrophobic dielectric surface.

C. Retroreflection Results

The retroreflection input angle, as a function of the light source's incident angle, is shown in Fig. 7. A 10:1 contrast is not achieved, and about 4:1 contrast is achieved only out to ±15°. This reduction in contrast is due to light leakage through the hydrophilic grid, and because the a_{MD}^2 loss should increase significantly with input angle. The maximum input angle at 30% of maximum reflection ($\theta_{30\%}$) is 30–35°. The external electrowetting light valve retroreflector has several material layers that light must traverse. This leads to a theoretical single pass transmission $T \sim 83.3\%$. Also, the aperture is only ~70% in the on state, leading to a maximum value of 49% for a_{MD}^2. As a result, the total retroreflective efficiency is $\eta(\%) = 12\%$.

D. Discussion

The external electrowetting light valve provides sufficiently low operating voltage (15 V), a low energy per switch (~7 mJ/m^2), and rapid switching of ~10–100 ms. The requirement of several material layers and a_{MD}^2 loss leads to an overall low optical efficiency. The off state light leakage provides low contrast (can be improved with a black pixel grid). As with most electrowetting devices, fabrication is scalable to large area on flexible substrates [20]. Because the retroreflective efficiency, contrast, and maximum input angle are rather poor in comparison to other approaches, a preliminary attempt was made to integrate the light valve into the corner cube itself, especially to reduce a_{MD}^2 optical loss (next section).

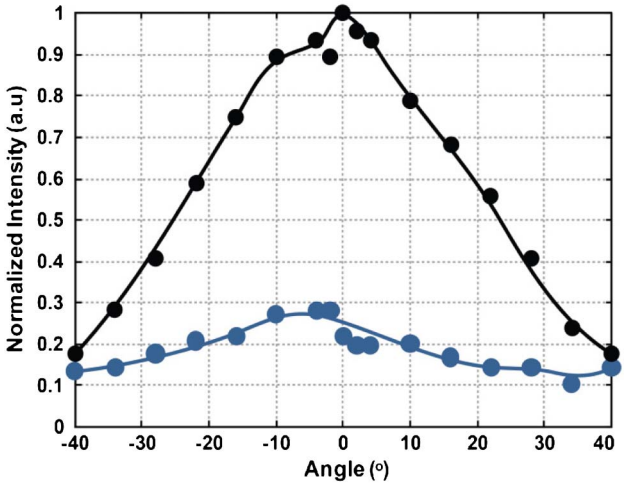

Fig. 7. (Color online) Retroreflection as a function of input angle for the external electrowetting light valve retroreflector. Both states of operation are plotted. Points are experimental data, and trend curves are for guidance.

7. Integrated Electrowetting Light Valve

Integration of the light valve into the corner cube structure was investigated to provide lower optical loss and a thinner overall form factor.

A. Construction and Fabrication

The integrated electrowetting light valve is shown in Fig. 8, where the light valve is vertically inverted and placed into the corner cube structure itself. One less substrate is needed, and the device can remain substantially thinner and more flexible. Construction consists of a glass or PET substrate coated with a transparent electrode and a hydrophobic dielectric. The bottom substrate is an array of microreplicated corner cubes coated with a reflective electrode (Al). To allow ease of fabrication, the larger 800 μm corner cubes were utilized. The hydrophilic pixel grid [Fig. 5(a)] is no longer needed, as the top ridges of the corner cube pixelate the oil into discrete volumes. The technique used for liquid dosing is unique. Water is applied onto the corner cube substrate. The water

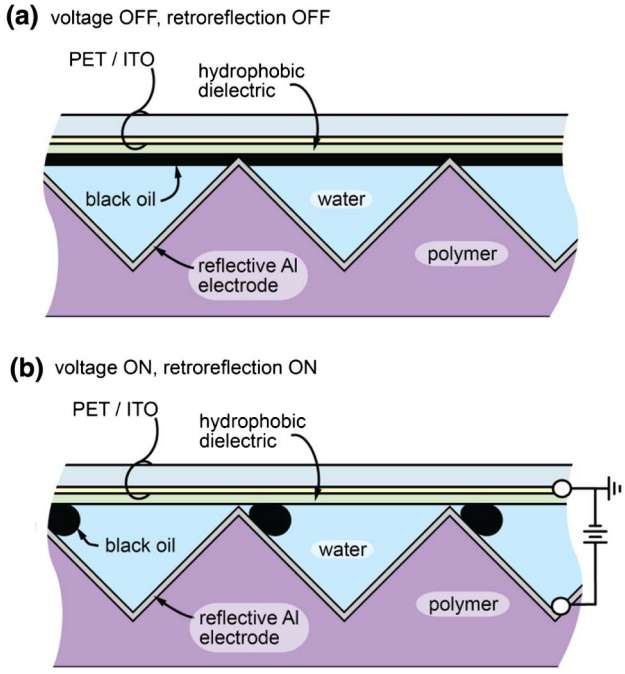

Fig. 8. (Color online) Integrated electrowetting light valve: (a) voltage off and light absorbing state, (b) voltage on and retroreflecting state.

is slowly advanced over the substrate to avoid air trapping and a vacuum degas can be used to remove any entrapped air bubbles. Next, a drop of dyed oil and the electrowetting top plate are placed onto the corner cube substrate. The hydrophobic surface of the top plate allows the oil to spread over the entire surface. For this device test, blue oil was used because it also allows visualization of the corner cubes beneath the oil.

B. Electrical Switching

Figures 8(a) and 9(a) show the off state of the device, whereby the oil film covers the corner cube input aperture and absorbs light (if black oil were used, all visible light would be absorbed). When electrically powered, there is a charge buildup that commences at the top ridges of the hydrophilic Al electrode. The water then wets the hydrophobic dielectric surface of the top substrate, displacing the oil from all directions, forming it into a spherical cap. The oil sphere quickly migrates to one of the corners of the corner cube, as can be seen in Figs. 8(b) and 9(b). When the voltage is released, the water recedes and the oil moves back into its original place.

C. Retroreflection Results

The single biggest advantage for integrating the colored oil into the corner cubes is the displacement of oil into the corners. The corners already contain the optically dead area (Fig. 1), and therefore most of the retroreflective aperture is active ($a_{MD} \approx 90\%$). Furthermore, with a thinner oil film and smaller oil droplets in the on state, the a_{MD}^2 loss can likely be completely eliminated. However, the fabrication method does not yet provide a large area with uniform oil dosing, and the available area for testing (Fig. 8) is too small for angular measurements. The maximum input angle should be only slightly less than a regular corner cube retroreflector film [Fig. 1(d)] and the on/off contrast should be $>10:1$ because there is no retroreflective light leakage path, as discussed for Fig. 6 (the external light valve).

As this device has very few materials that light must transmit through, its optical efficiency will be very high, with a calculated single pass transmission of $T = 89.8\%$. Along with an active area (a_{MD}) of 90%, the calculated optical efficiency is $\eta(\%) = 23\%$.

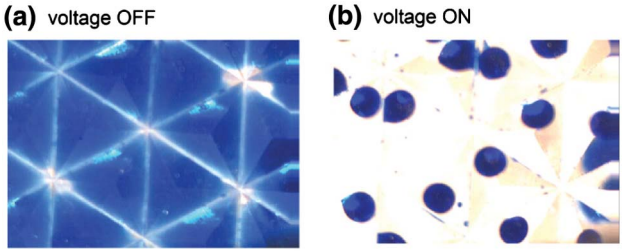

Fig. 9. (Color online) Collinear images of the integrated electrowetting light valve retroreflector in its (a) off state and (b) on state. Blue oil was used instead of black oil to aid visualization of the retroreflector below the oil film.

D. Discussion

The internal (integrated) electrowetting light valve has all the advantages of the external light valve, plus it has the advantage of high retroreflective efficiency. Furthermore, the integrated approach can lead to a very thin form factor requiring only two substrates.

8. Conventional Liquid Crystal Light Valve

Liquid crystal displays are widely available and therefore are highly appropriate for investigation with switchable retroreflection.

A. Construction and Fabrication

The liquid crystal light valve and retroreflector are diagrammed in Fig. 10. For this work, we used a standard twisted nematic liquid crystal display (TNLCD) over a corner cube retroreflective film. Details of the TNLCD fabrication can be reviewed in numerous publications [28–31]. The TNLCD is simply adhered to the retroreflective film.

B. Electrical Switching

Detailed operation of the liquid crystal light valves can be found elsewhere [28–31]. At zero voltage, the

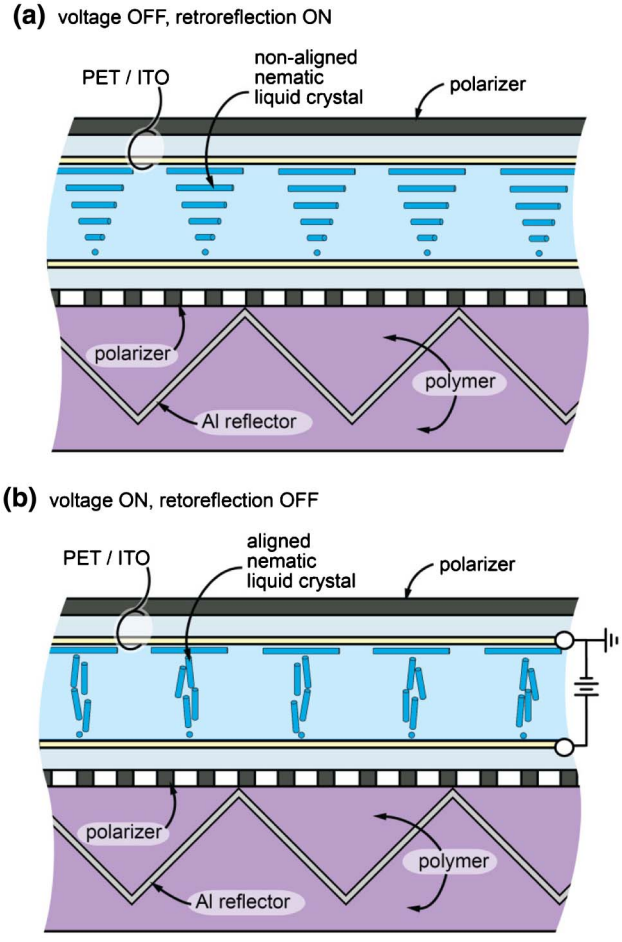

Fig. 10. (Color online) Liquid crystal light valve retroreflector in the (a) retroreflecting state with no voltage applied, (b) light absorbing state with voltage applied.

liquid crystal molecules are aligned with each plate and rotate the polarization of light such that light is able to transmit through the crossed polarizers [Figs. 10(a) and 11(a), retroreflection]. When voltage is applied, the liquid crystal molecules align with the electric field; no polarization rotation occurs, and the light is absorbed due to the crossed polarizers [Figs. 10(b) and 11(b)]. Unlike the previously described approaches, this device is retroreflective with zero voltage. However, the polarizers can instead be applied in optical alignment, and the device could instead be opaque with zero voltage.

C. Retroreflection Results

The achievable input angles are plotted in Fig. 12. This device has a maximum contrast of 600∶1 with nearly 100∶1 over its entire field of view (though erratic). The maximum input angle $\theta_{30\%}$ is 35°.

This device has a substantial loss in optical efficiency due to the material layers. This is mostly due to the polymer sheet polarizers which typically have a transmittance of only 38% [32]. Also, after retroreflecting, the proper polarization of light for efficient return is lost [33], and will again be filtered out by the polarizer. Polarizer aside, this device also has numerous layers, including three adhesive layers (polarizers and retroreflective film). This leads to a theoretical single-pass transmission (T) of about 35.2%, the lowest of all of those reviewed. It does, however, have a 100% device active area (a_{MD}). With the standard retroreflective film efficiency, the total efficiency ($\eta(\%)$) of this device is about 4%.

D. Discussion

LCDs are currently widely used in low-cost and low-power devices, and have an operation voltage of <5 V. Their spectral range covers the entire visible spectrum, and switching can be seen over a wide input angle with high contrast. LCDs are currently manufactured in much larger than 100 cm^2 areas. The device has the lowest retroreflection of all those reviewed due to the polarizers. Therefore, an alternate liquid crystal device not utilizing polarizers was investigated (next section).

9. Liquid Crystal Scattering

Liquid crystal scattering exploits the birefringent nature of liquid crystals when randomly oriented in a polymer matrix. As a result an optical diffuser can

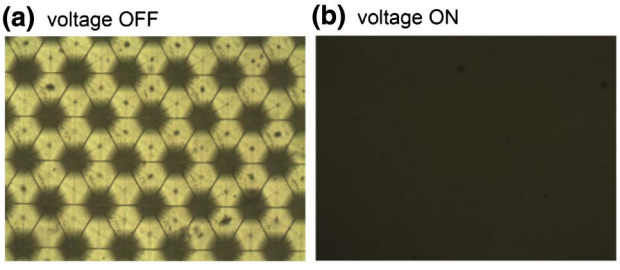

Fig. 11. (Color online) Collinear images of liquid crystal light valve retroreflector in the (a) voltage off and (b) voltage on states.

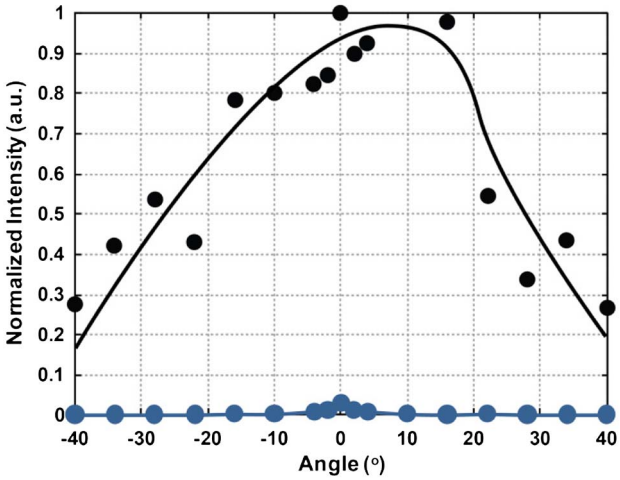

Fig. 12. (Color online) Retroreflection as a function of input angle for the TNLCD retroreflector. Both states of operation are plotted. Points are experimental data, and trend lines are for guidance.

be electrically switched to be optically transparent, similar to that discussed for the integrated electrowetting lenslet.

A. Construction and Fabrication

Liquid crystal scattering is performed by use of a PDLC shutter adhered to a retroreflective film, as

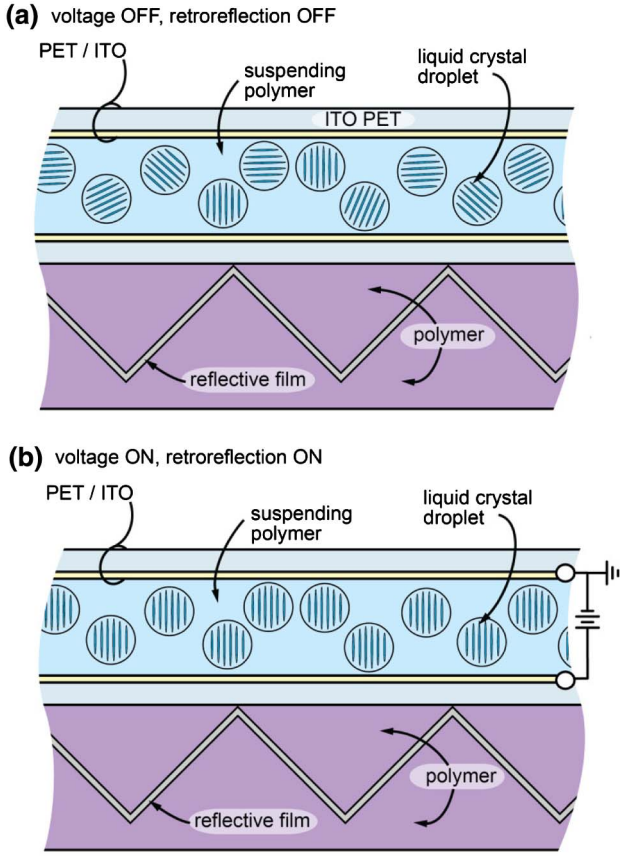

Fig. 13. (Color online) Polymer dispersed liquid crystal retroreflector in the: (a) voltage off state and scattering state; (b) voltage on and retroreflecting state.

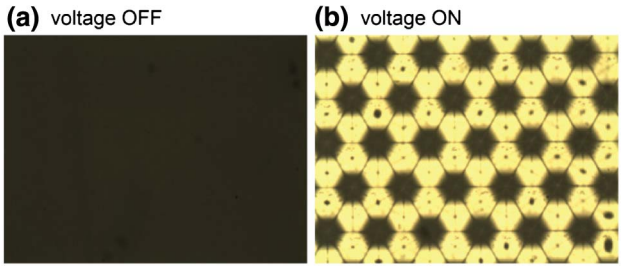

Fig. 14. (Color online) Collinear images of the polymer dispersed liquid crystal scattering retroreflector in its (a) voltage off state and (b) voltage on state.

can be seen in Fig. 13. PDLC shutters have been extensively researched and fabrication can be reviewed in numerous publications [34–37].

B. Electrical Switching

Detailed description of operation for the switching mechanisms of the PDLC modulator can be found elsewhere [34–37]. With no voltage applied, the polymer suspended liquid crystal droplets are randomly oriented with respect to the primary optical axis, as can be seen in Fig. 13(a). This creates a random difference in refractive index that incident light will encounter, which causes the light to scatter, and the device appears optically diffuse [no retroreflection, Fig. 14(a)]. When the device is electrically powered, the liquid crystal droplets orient themselves to be aligned with the electric field [Figs. 13(b) and 14(b)]. This allows for a match in refractive index with the suspending polymer, and the PDLC layer becomes transparent, thus allowing retroreflection. When the voltage is turned off, the device reverts back to its diffuse state.

C. Retroreflection Results

The PDLC device has excellent switching capabilities, and a maximum input angle $\theta_{30\%}$ of ~40° can be seen in Fig. 15. A contrast of >10:1 is also maintained out to ~ ± 40°. There are several irregular features in the angular dependence that are currently not understood, but overall the retroreflective performance is comparable to a bare retroreflective film.

The liquid crystal scattering retroreflector has few material layers and subsequently lower optical loss, with a single-pass transmission (T) of about 85%. The device has no loss in modulation device active area ($a_{\mathrm{MD}} = 100\%$) and with the retroreflective film efficiency applied, it comes out to a total efficiency of $\eta(\%) = 25\%$.

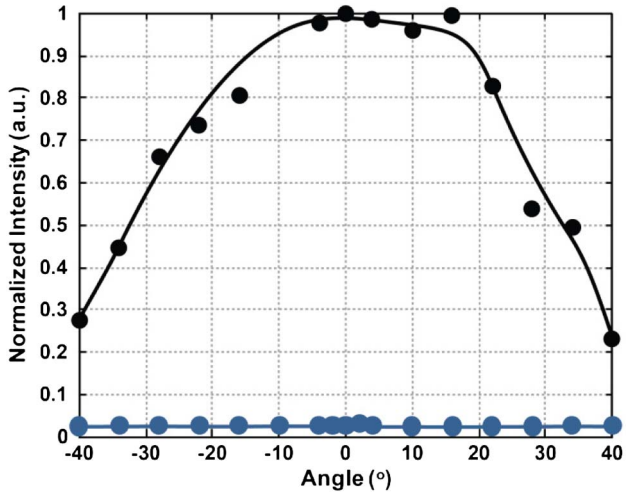

Fig. 15. (Color online) Retroreflection as a function of input angle for the polymer-dispersed liquid crystal retroreflector. Both states of operation are plotted. Points are experimental data, trend lines are for guidance.

D. Discussion

Operating voltage greatly depends on the PDLC's composition and thickness, and can be as low as 5 V [36]. Energy per switch (~1.3 mJ/m^2) is low, and switching speeds of <2 ms [37] have been observed. The films tested herein switched with a rise time of <2 ms with a fall time of <30 ms. The spectral range covers the entire visible spectrum and into night-vision IR, and boasts a wide input angle with good contrast. A large reflection area is also achievable on thin and flexible materials. Optical efficiency is high because no polarizers are used. The required fabrication process is also one of the simplest of those reviewed herein.

10. Discussion, Conclusions, and Demonstration

The devices discussed herein are all viable technologies to be used for switchable retroreflectors for human eye conspicuity applications. TNLCD and the external electrowetting light valve, however, do not meet all of the ideal performance metrics set in the introduction. Table 2 provides a summary of performance for all tested devices. The electrowetting lenslet retroreflector provides the highest optical efficiency, followed closely by the PDLC retroreflector, and then the integrated electrowetting light valve. The overall conclusions are as follows: The integrated electrowetting lenslet has the highest performance of all approaches tested, including the potential for the fastest switching speed. Higher speed may be

Table 2. Comparison of Key Attributes of the Five Types of Switchable Retroreflectors

	EW Lenslet	External EW Light Valve	Integrated EW Light Valve	TNLC	PDLC
Efficiency $\eta(\%)$	27%	12%	23%	4%	25%
Maximum input angle	±35	±30	not measured	±35	±38
Contrast	>10:1	5:1	not measured	>100:1	40:1
Operating voltage	5	10	10	<5	25
Energy per switch (mJ/m^2)	~1.8	~7.0	~9.5	~1.2	~1.3

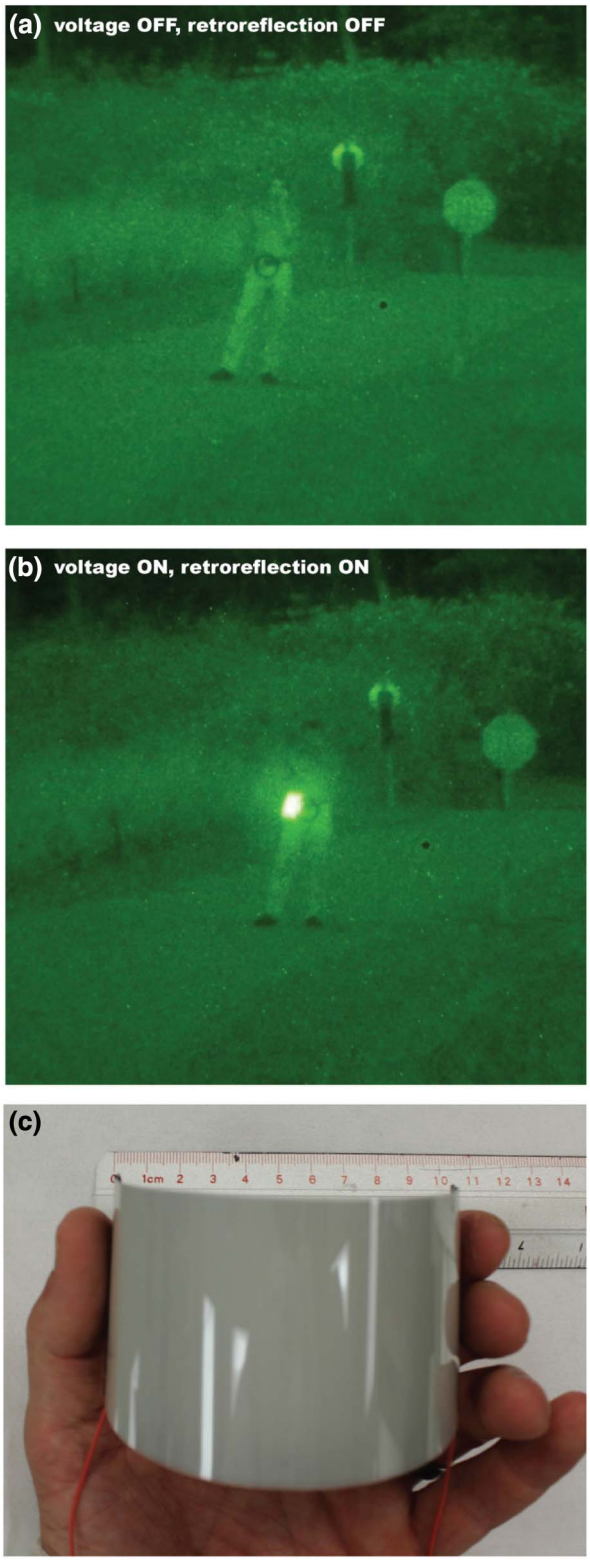

Fig. 16. (Color online) Field demonstration of a switchable retroreflector using night vision through binoculars at a range of 200 m with (a) no voltage applied/tag off and (b) voltage applied/tag on. The author J. Heikenfeld is holding and modulating the tags while authors P. Schultz and B. Cumby illuminate with a 28 mW source spread to 2 m diameter and take photographs through night vision goggles. (c) Image of an ~5 × 15 cm switchable retroreflector being bent to about a 10 cm diameter.

useful for additional data transfer or lock-in amplification of the detected retroreflection signal. The PDLC device is second in overall performance mainly because of slower switching speed. However, PDLC films can be easily obtained commercially, and therefore PDLC initially is a more attractive approach for switchable retroreflectors. PDLC films are currently operable from −10 to 60 degrees Celsius, but with alternate chemistries can be extended to −40 to 100 degrees Celsius [38]. The use of PET substrates with proper sealing and electrode isolation allows for a high impact resistant device that is operable in harsh environments, including rain and dust.

With the PDLC chosen over the other switching mechanisms, a full night and day demonstration with a PDLC retroreflector was performed. As shown in Figs. 16(a) and 16(b), a ~5 × 15 cm device is easily visualized at 200 m at night, using conventional AN/PVS14 night-vision goggles and a 28 mW 850 nm source spread to ~2 m diameter. Night vision was tested, as it is emerging in automotive vision and safety systems. During the day, 400 m viewing distance has also been validated with a 30 mW 532 nm laser pointer. The fabricated devices are highly flexible [Fig. 16(c)], with bend radii of <5 cm demonstrated. For visible and night-vision conspicuity applications, switchable retroreflectors are now proven as feasible based on use of electrowetting lenslets or polymer-dispersed liquid crystals.

The authors would like to thank S. Scott of Reflexite Inc. for providing corner cube templates.

References

1. L. Zhou, J. M. Kahn, and K. S. J. Pister, "Corner-cube retroreflectors based on structure-assisted assembly for free-space optical communication," J. Microelectromech. Syst. **12**, 233–242 (2003).
2. J. B. Stewart, D. Freedman, S. Cornelissen, M. N. Horenstein, P. Woskov, and J. Tang, "Low power MEMS modulating retroreflectors for optical communication," Libr. Acquis. Pract. Theory **7595**, 759505 (2010).
3. G. C. Gilbreath, W. S. Rabinovich, T. J. Meehan, M. J. Vilcheck, R. Mahon, R. Burris, M. Ferraro, I. Sokolsky, J. A. Vasquez, C. S. Bovais, K. Cochrell, K. C. Goins, R. Barbehenn, D. S. Katzer, K. Ikossi-Anastasiou, and M. J. Montes, "Large-aperture multiple quantum well modulating retroreflector for free-space optical data transfer on unmanned aerial vehicles," Opt. Eng. **40**, 1348–1356 (2001).
4. W. S. Rabinovich, P. G. Goetz, R. Mahon, L. Swingen, J. Murphy, M. Ferraro, H. R. Burris, C. I. Moore, M. Suite, G. C. Gilbreath, S. Binari, and D. Klotzkin, "45-Mbit/s cat's-eye modulating retroreflectors," Opt. Eng. **46**, 104001 (2007).
5. M. Plett, W. S. Rabinovich, R. Mahon, M. S. Ferraro, P. G. Goetz, C. I. Moore, and W. Freeman, "Free-space optical communication link across 16 kilometers over the Chesapeake Bay to a modulated retroreflector array," Opt. Eng. **47**, 045001 (2008).
6. J. Lloyd, "A brief history of retroreflective sign face sheet materials," http://www.rema.org.uk/pdf/history-retroreflective-materials.pdf.
7. S. Winburn, A. Baker, and J. Leishman, "Angular response properties of retroreflective screen materials used in wide-field shadowgraphy," Exp. Fluids **20**, 227–229 (1996).
8. MinimumReflectivity.org, http://www.minimum reflectivity .org/retroreflective.asp.
9. H. D. Eckhardt, "Simple model of corner reflector phenomena.," Appl. Opt. **10**, 1559–1566 (1971).

10. Reflexite, http://www.reflexite.com.
11. 3m Corporation, http://www.3m.com.
12. F. E. Nicodemus, "Directional Reflectance and Emissivity of an Opaque Surface," Appl. Opt. **4**, 767–773 (1965).
13. S. C. Pont and J. J. Koenderink, "Bidirectional reflectance distribution function of specular surfaces with hemispherical pits," J. Opt. Soc. Am. A **19**, 2456–2466 (2002).
14. A. B. Marchant, K. D. Jeppson, and R. T. Scott, "Conspicuity tape for enhanced laser range finding," Opt. Eng. **49**, 046401 (2010).
15. J. Heikenfeld, P. Drzaic, J.-S. Yeo, and T. Koch, "Review Paper: A critical review of the present and future prospects for electronic paper," J. Soc. Inf. Disp. **19**, 129–156 (2011).
16. F. Mugele and J.-C. Baret, "Electrowetting: from basics to applications," J. Phys. Condens. Matter **17**, R705–R774 (2005).
17. P. G. De Gennes and J. Prost, *The Physics of Liquid Crystals* (Oxford University, 1995), p. 597.
18. V. G. Chigrinov, *Liquid Crystal Devices: Physics and Applications* (Artech, 1999), p. 366.
19. S.-T. Wu and D.-K. Yang, *Fundamentals of Liquid Crystal Devices* (Wiley, 2006), p. 394.
20. K. Zhou, J. Heikenfeld, K. A. Dean, E. M. Howard, and M. R. Johnson, "A full description of a simple and scalable fabrication process for electrowetting displays," J. Micromech. Microeng. **19**, 065029 (2009).
21. N. R. Smith, D. C. Abeysinghe, J. W. Haus, and J. Heikenfeld, "Agile wide-angle beam steering with electrowetting microprisms.," Opt. Express **14**, 6557–6563 (2006).
22. M. K. Kilaru, B. Cumby, and J. Heikenfeld, "Electrowetting retroreflectors: Scalable and wide-spectrum modulation between corner cube and scattering reflection," Appl. Phys. Lett. **94**, 041108 (2009).
23. M. K. Kilaru, J. Yang, and J. Heikenfeld, "Advanced characterization of electrowetting retroreflectors.," Opt. Express **17**, 17563–17569 (2009).
24. S. Kuiper and B. H. W. Hendriks, "Variable-focus liquid lens for miniature cameras," Appl. Phys. Lett. **85**, 1128–1130 (2004).
25. R. A. Hayes and B. J. Feenstra, "Video-speed electronic paper based on electrowetting," Nature **425**, 383–385 (2003).
26. B. Sun and J. Heikenfeld, "Observation and optical implications of oil dewetting patterns in electrowetting displays," J. Micromech. Microeng. **18**, 025027 (2008).
27. A. Schultz, J. Heikenfeld, H. Kang, and W. Cheng, "1000:1 contrast ratio transmissive electrowetting displays," J. Disp. Technol. **7**, 583–585 (2011).
28. M. Schadt, "Voltage-dependent optical activity of a twisted nematic liquid crystal," Appl. Phys. Lett. **18**, 127–128 (1971).
29. J. Fergason, "Display devices utilizing liquid crystal light modulation," U.S. patent 3731986 (8 May 1973).
30. M. Gu, "The world of liquid crystal displays," http://www.personal.kent.edu/~mgu/LCD/tn.htm.
31. G. W. Gray and S. M. Kelly, "Liquid crystals for twisted nematic display devices," J. Mater. Chem. **9**, 2037–2050 (1999).
32. Edmund Optics, "Visible linear polarizing laminated film," http://www.edmundoptics.com/products/displayproduct.cfm?productid=1912.
33. S. E. Segre and V. Zanza, "Mueller calculus of polarization change in the cube-corner retroreflector.," J. Opt. Soc. Am. A **20**, 1804–1811 (2003).
34. P. S. Drzaic, "Polymer dispersed nematic liquid crystal for large area displays and light valves," J. Appl. Phys. **60**, 2142–2148 (1986).
35. J. W. Doane, A. Golemme, J. L. West, J. B. Whitehead, and B. G. Wu, "Polymer dispersed liquid crystals for display application," Mol. Cryst. Liq. Cryst. **165**, 511–532 (1988).
36. G. Spruce and R. D. Pringle, "Polymer dispersed liquid crystal (PDLC) films," Electron. Commun. Eng. J. **4**, 91–100 (1992).
37. L. Petti, P. Mormile, and W. J. Blau, "Fast electro-optical switching and high contrast ratio in epoxy-based polymer dispersed liquid crystals," Opt. Lasers Eng. **39**, 369–377 (2003).
38. J. L. West, "Extended temperature range polymer dispersed liquid crystal light shutters," U.S. patent 5004323 (2 April 1991).